

Level-crossing spectroscopy of the 7, 9, and 10D_{5/2} states of ¹³³Cs and validation of relativistic many-body calculations of the polarizabilities and hyperfine constants

M. Auzinsh,^{1,*} K. Blushs,¹ R. Ferber,¹ F. Gahbauer,¹
 A. Jarmola,¹ M. S. Safronova,² U. I. Safronova,³ and M. Tamanis¹

¹*Department of Physics and Mathematics, University of Latvia, Rainis Blvd. 19, Riga LV-1586, Latvia*

²*Department of Physics and Astronomy, 223 Sharp Lab,
 University of Delaware, Newark, Delaware 19716*

³*Physics Department, University of Nevada, Reno, Nevada 89557*

(Dated: September 2, 2018)

We present an experimental and theoretical investigation of the polarizabilities and hyperfine constants of D_J states in ¹³³Cs for $J = 3/2$ and $J = 5/2$. New experimental values for the hyperfine constant A are obtained from level-crossing signals of the (7,9,10)D_{5/2} states of ¹³³Cs and precise calculations of the tensor polarizabilities α_2 . The results of relativistic many-body calculations for scalar and tensor polarizabilities of the (5-10)D_{3/2} and (5-10)D_{5/2} states are presented and compared with measured values from the literature. Calculated values of the hyperfine constants A for these states are also presented and checked for consistency with experimental values.

PACS numbers: 32.10.Dk,32.10.Fn,31.15.Ar,31.25.Jf

I. INTRODUCTION

Level-crossing spectroscopy in an electric field has been shown to be a useful technique to determine atomic properties. Already the first experimental studies of resonant signals at pure electric field crossings of magnetic $\pm m_F$ components of certain hyperfine (hfs) atomic levels F at nonzero electric field [1, 2, 3] and their further development by applying two-step laser excitation [4] demonstrated how this technique could be used to obtain atomic properties. The method makes use of the fact that the electric field values at which magnetic sub-levels m_F cross in an electric field depend on the tensor polarizability α_2 and on the hfs constants. When the electric field is scanned and laser induced fluorescence (LIF) of definite polarization is observed, these crossings are associated with resonance behavior in the LIF signals. When the separation between crossings is large compared to the widths of the resonance signals, as in the $nD_{3/2}$ states of the ¹³³Cs atom (see Fig. 1a), they lead to rather well-pronounced resonances in the observed fluorescence. Moreover, these resonances correspond exactly to the level-crossing points under appropriate experimental conditions. Such resonances were used to measure the tensor polarizabilities α_2 in the 7, 9D_{3/2} states of ¹³³Cs atoms [4], in which the magnetic dipole coupling hfs constant A had been previously measured with good precision, and the electric quadrupole hfs constant B was assumed to be negligibly small [5].

Such measurements become more challenging, however, in the case of the $nD_{5/2}$ states of cesium, since there are many closely spaced crossing points of magnetic $\pm m_F$ components (see Fig. 1,b-d). As a result,

the level-crossing signals overlap and no longer contain discernable resonances. In this case, reliable values for atomic properties can be extracted only by means of a very detailed and accurate theoretical description of the observed electric field dependence of the signals as a function of atomic properties and experimental conditions. Such theoretical descriptions have been developed and tested in connection with the $nD_{3/2}$ states [4]. Nevertheless, the level-crossing technique cannot be used at this time to improve the knowledge of the tensor polarizabilities α_2 of the $nD_{5/2}$ states because the extant measurements of the hfs constant A contain uncertainties on the order of 30%. The small hyperfine interaction, especially for $n > 7$, makes them difficult to measure [6, 7].

The first value of the hfs constant A of the $nD_{5/2}$ states of ¹³³Cs was obtained with measurements of the widths of optical double resonance (ODR) signals in the Paschen-Back region. The results for the 9D_{5/2} and 10D_{5/2} states were $-0.5(2)$ MHz and $-0.4(2)$ MHz, respectively [8]. These values were improved through level-crossing spectroscopy in magnetic fields, yielding $-0.40(15)$ and $-0.30(10)$ MHz [6]. The authors combined these data with previous ODR measurements [7] and presented the weighted average as $-0.45(10)$ and $-0.35(10)$ MHz. They concluded that the quadrupole interaction can be completely ignored when fitting the experimental data. For the 7D_{5/2} state, Bulos *et al.* estimated the A value to be $-1.7(2)$ MHz from the ODR signal width [9]. The drawback of the ODR experiments on the 7,9,10D_{5/2} signals is that it is necessary to use indirect cascade transitions to observe the $nD_{5/2}$ signals because of the presence of scattered light at the $nD_{5/2} \rightarrow 6P_{3/2}$ fluorescence transition [7, 9].

The tensor polarizabilities α_2 for the $nD_{5/2}$ states in cesium under discussion are known with far greater precision. For the 10D_{5/2} state, α_2 has been measured by Xia and coworkers to a very high precision of about 0.3% at

*Electronic address: mauzins@latnet.lv

$6815(20) \times 10^3$ a.u. [10]. For the $9D_{5/2}$ state the α_2 value is measured with ca. 5% accuracy at $2650(140) \times 10^3$ a.u. by means of level crossing spectroscopy in combined electric and magnetic fields [6, 11]. For the $7D_{5/2}$ state, there exists a measured value of $129(4) \times 10^3$ a.u. presented in Ref. [12], which, however, should be verified, because it differs significantly from the theoretical value of 140×10^3 a.u. [13]. Furthermore, a more recent measurement of α_2 for the $7D_{3/2}$ state [4] was closer to the theoretical estimate of [13] than the measurement of [12].

The situation with the electronic structure calculations is similar to the experimental situation. Rather good accuracy has been achieved for theoretical estimates of the tensor polarizability α_2 , as can be seen from the fact that the calculations of [13] for ^{133}Cs agree with very accurate experimental data for the $(10-13)D_{3/2,5/2}$ states [10]. Despite this precision for the polarizability, the estimates of the hfs constants are poor and can hardly be evaluated reliably, for reasons that will be discussed below. Therefore, there is a need for more accurate values for the hfs constants of the $nD_{5/2}$ states.

In order to determine the hfs constants A from our measurements of m_F sublevel crossing signals in the $7,9,10D_{5/2}$ states of cesium, we used the following approach. We fit the measured signals with calculated curves derived from simulations, which had been developed and tested in [4]. With the tensor polarizability α_2 fixed, these fits yielded the hfs constant A . To choose the proper value for α_2 , we performed an all-order relativistic many-body calculation.

Section II contains a description of the experiment, followed by a discussion of the simulations used to describe the measured signals. The all-order relativistic many-body calculations that provided the values for the tensor polarizabilities α_2 are described in section III, and the values for α_2 obtained from these calculations are compared with earlier experimentally measured values. In section IV we discuss the application of these calculations to estimating the hfs constants and compare them to the results of previous experiments. In section V we show how to use our experimental results from section II and the calculated tensor polarizabilities from section III to estimate new values for the hfs constant A .

II. EXPERIMENT AND DESCRIPTION OF SIGNALS

A. Method

The premise of level crossing spectroscopy is that the spatial intensity distribution and polarization of the laser induced fluorescence produced when an atom is excited depends on the coherences between different magnetic sublevels m_F of hyperfine levels F . Such coherences are destroyed when the degeneracy between different sublevels is broken in an electric field. However, in the case of linear polarization, they can be restored when sublevels

with $\Delta m_F = \pm 2$ cross at certain electric field values. Figure 1 shows the hyperfine level-splitting diagram in an external electric field for the $7D_{3/2}$ and $7D_{5/2}$ states of cesium. This diagram is calculated by diagonalizing the Hamiltonian, which includes the hyperfine and Stark interactions, in an uncoupled basis [14].

When applying the method of level crossing spectroscopy to the study of the $nD_{5/2}$ states of cesium, one encounters two difficulties not present in the case of the $nD_{3/2}$ states. The first difficulty is that the $nD_{5/2}$ hyperfine manifold contains seven level crossings with $\Delta m_F = \pm 2$, whereas the $nD_{3/2}$ manifold contains only two (see Fig. 1). The large number of level crossings in the $nD_{5/2}$ state wash out the sharp resonances that could be observed in the $nD_{3/2}$ state.

The second difficulty is that in the case of the $nD_{5/2}$ states, after the two-step excitation $6S_{1/2} \rightarrow 6P_{3/2} \rightarrow nD_{5/2}$ (see Fig. 2), it is necessary to observe the fluorescence from the $nD_{5/2} \rightarrow 6P_{3/2}$ transition. Thus, scattered light from the exciting laser constitutes a high background that must be suppressed. Figure 2 shows the level excitation scheme.

B. Experimental details

We studied cesium vapor at room temperature in a glass cell. The experimental setup is essentially the same as in Ref. [4]. We could apply an electric field between two transparent electrodes inside the cell, which were separated by a 2.5 mm gap. Figure 3 shows a schematic diagram of the experimental setup and geometry. The most crucial detail of the experiment is the relative orientation of the electric field and the polarization vectors of the linearly polarized laser radiation. The first laser, which excited the $6S_{1/2} \rightarrow 6P_{3/2}$ transition, was polarized with its polarization vector \mathbf{E}_1 parallel to the dc electric field \mathcal{E} , which was along the z -axis. The second laser, which excited the $6P_{3/2} \rightarrow 7,9,10D_{5/2}$ transition, was sent in a counter propagating direction and was polarized perpendicular to the first, with polarization vector \mathbf{E}_2 parallel to the y -axis. We observed the laser induced fluorescence (LIF) at the $nD_{5/2} \rightarrow 6P_{3/2}$ transition along the z -axis through the transparent electrodes. A linear polarizer selected the intensities of the LIF polarization components along the x or y -axes I_x or I_y . Since the LIF was observed at the same frequency at which the second laser was operating, it was necessary to suppress carefully the scattered light by means of diaphragms. The scattered light accounted for between 30% and 50% of the measured signal. We checked that this background remained stable during the measurements and subtracted it from the signals. The LIF passed through an MDR-3 monochromator with 2.6 nm/mm inverse dispersion and was recorded with a PMT in photon counting mode during one second time intervals.

The first laser was always a diode laser (based on an LD-0850-100sm laser diode) and was tuned to excite the

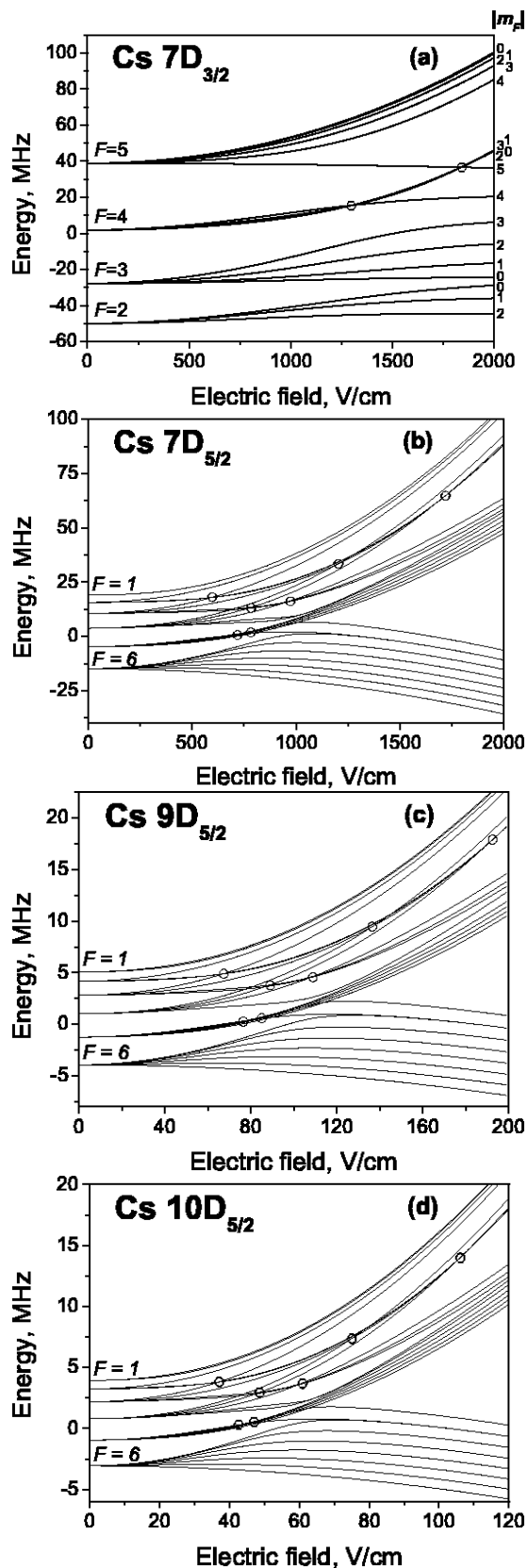


FIG. 1: Hyperfine level-splitting diagram in an external electric field for the (a) $7D_{3/2}$, (b) $7D_{5/2}$, (c) $9D_{5/2}$, and (d) $10D_{5/2}$ states of Cs. Circled points indicate level crossings with $\Delta m_F = \pm 2$.

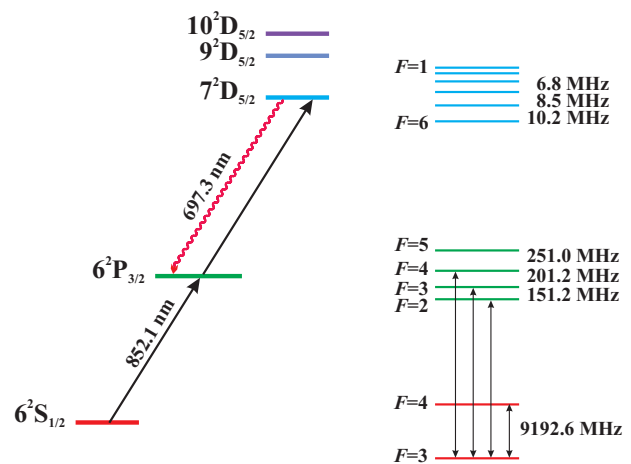


FIG. 2: Level excitation scheme.

$6^2P_{3/2}$ state from the $F = 3$ hfs component of the ground state. We chose to excite from the $F = 3$ level, because in this way we could avoid the $F = 6$ level of the $nD_{5/2}$ final state. The $F = 6$ level contained no level crossings and thus would contribute only background. We took advantage of a sideband of the radiation of the first laser in order to achieve broadband excitation.

For the second excitation step, we used a diode laser (based on a Hitachi HL6738MG laser diode) in the case of the $7D_{5/2}$ state and a CR699-21 ring dye laser with Rhodamine 6G dye in the case of the $9D_{5/2}$ and $10D_{5/2}$ states. The second laser was operated in single mode regime. We recorded data at different values of the detuning of the second laser in order to compare the results obtained at different detunings with simulations. A HighFinesse WS/6 wavemeter allowed us to measure changes in the lasers' detuning with a resolution of 30 MHz. However, in general we operated at the detuning that maximized the fluorescence signal. When the second laser was the diode laser, we jittered its output frequency over a range of approximately 1.2 GHz by applying a sawtooth wave with a frequency of tens of Hertz to a piezoelectric crystal mounted to its feedback grating. The laser power was of the order of a few mW, and the laser beam diameters were approximately 1 mm.

The electric field produced in the cell was calibrated with measurements of level-crossing signals for the $10D_{3/2}$ state of cesium as in [4]. The level-crossing resonance positions obtained with our cell were compared with the crossing points calculated from the tensor polarizability of [10] and the hfs constant A of [5]. The overall uncertainty on the electric field magnitude was estimated to be about 1%.

C. Experimental results

We plot with markers the measured LIF intensity as a function of the electric field for the $nD_{5/2}$ states of cesium in Figures 4–6. Signals for different experimental

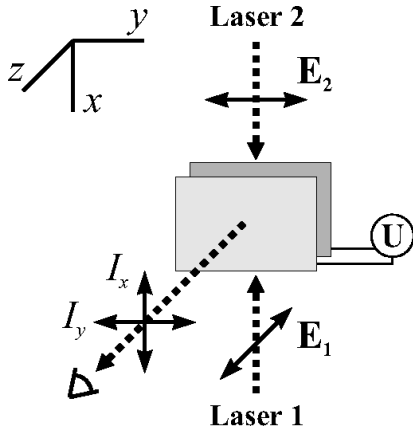
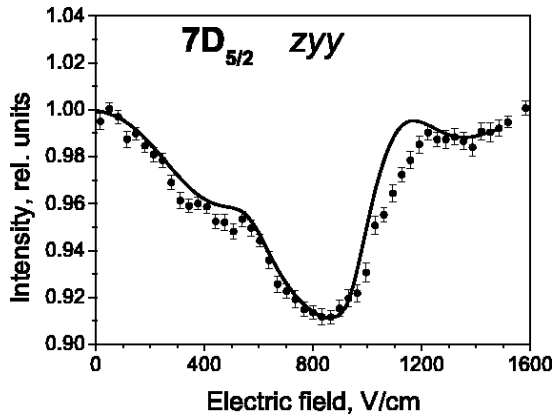
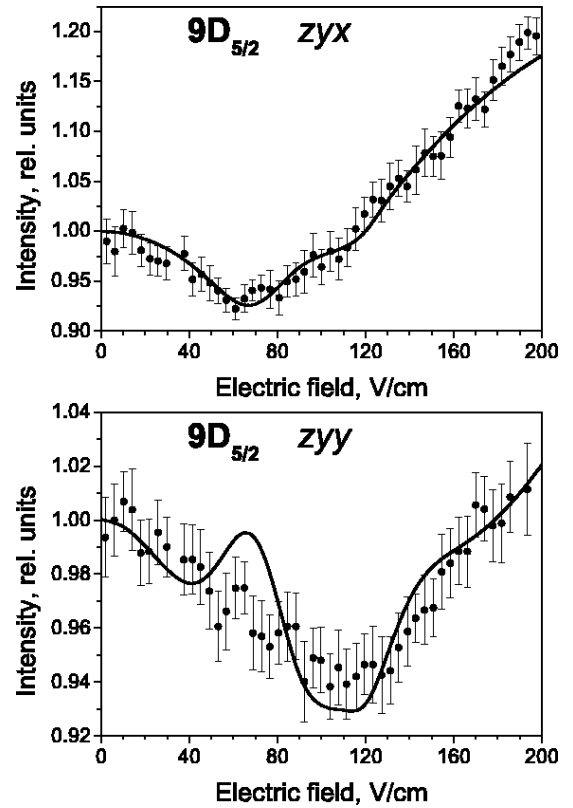
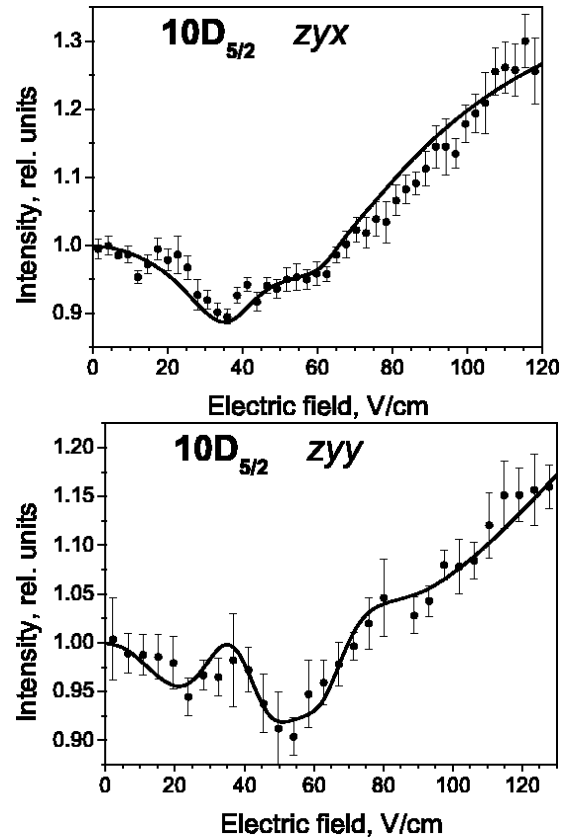


FIG. 3: Experimental geometry.

geometries are plotted. We label the experimental geometry as zyy or zyx , where the first and the second letters, z and y , denote the orientation of the polarization of the first and second lasers, $\mathbf{E}_1 \parallel z$ and $\mathbf{E}_2 \parallel y$, and the third letter, x or y , denotes the polarization direction of the observed LIF. The solid line in the figure indicates the results of the simulations that are described below. As inputs to the theoretical model, we used the tensor polarizabilities calculated with the relativistic many-body approach described in section III below.

FIG. 4: Experimental results for $7D_{5/2}$.

As can be seen from Figures 4, 5, and 6 there are no well-defined level crossing resonances. Nevertheless, a curve with multiple features is obtained, and these features can be fitted with the results of a simulation based on a theoretical model. This simulation is described in the following subsection. The fit involves adjusting the hyperfine constant A and those experimental parameters that we could not measure absolutely, such as the laser detuning. We fix the tensor polarizability α_2 at the values that are obtained from the calculations described in section III.

FIG. 5: Experimental results for $9D_{5/2}$.FIG. 6: Experimental results for $10D_{5/2}$.

D. Signal description

Since well-defined resonances are no longer present in the signals of the $D_{5/2}$ states, the data can be interpreted only by means of simulations based on a detailed model. Such a model was elaborated in detail and verified in a previous publication [4], so we will only outline the approach in what follows.

The model describes atoms that interact simultaneously with radiation produced by two lasers with relatively broad spectral profiles, which were necessary to excite coherently magnetic sublevels that are split by an external electric field \mathcal{E} (see Fig. 1). The model assumes that the atoms move classically and are excited at the internal transitions. Thus, the internal atomic dynamics can be described by a semiclassical atomic density matrix ρ , which also depends on the classical coordinates of the atomic center of mass.

The ground state of the Cs atom consists of two hyperfine levels with total angular momentum $F_g = 3$ and $F_g = 4$, each containing $2F_g + 1$ magnetic sublevels. The first laser excites the atoms from the ground state to the $6P_{3/2}$ state, which contains hyperfine levels $F_e = 2, 3, 4$, and 5. The second laser excites the atom from the $6P_{3/2}$ state to the $nD_{5/2}$ state, which contained hyperfine levels $F_f = 1, 2, 3, 4, 5$, and 6.

The external electric field \mathcal{E} partially decouples the electronic angular momentum from the nuclear spin, which implies that the magnetic sublevel energies no longer depend quadratically on the electric field (see Fig. 1). In order to obtain the real dependence on the electric field, it is necessary to diagonalize the full Hamiltonian matrix. It is also necessary to take into consideration that the decoupling of angular momentum from nuclear spin alters the dipole transition probabilities between magnetic sublevels.

The entire model is based on the Optical Bloch Equations (OBEs) for the density matrix ρ (see, for example, [15])

$$i\hbar \frac{\partial \rho}{\partial t} = [\hat{H}, \rho] + i\hbar \hat{R}\rho. \quad (1)$$

The relaxation operator \hat{R} includes spontaneous emission and transit relaxation. We assume that the density of atoms is sufficiently low that different velocity groups of thermally moving atoms do not interact. The elements of the relaxation matrix are given in [4]. The Hamiltonian $\hat{H} = \hat{H}_{hfs} + \hat{V}$ includes the hyperfine Hamiltonian and the dipole interaction operator $\hat{V} = -\hat{\mathbf{d}} \cdot \mathbf{E}(t)$, where $\hat{\mathbf{d}}$ is the electric dipole operator and $\mathbf{E}(t)$ is the electric field of the exciting radiation.

The equations can be simplified by assuming that each laser excites only the transition to which it is tuned. We also apply the rotating wave approximation for multi-level systems [16] to the OBEs. The resulting stochastic differential equations can be further simplified by using the decorrelation approach [17]. The stochasticity derives

from the random fluctuations of the laser radiation with finite spectral width. This approach assumes that both lasers are uncorrelated and that the integration time for each measurement is large compared to the characteristic phase-fluctuation time of the exciting light source. The decorrelation approximation amounts to solving the equations of the density matrix elements that correspond to optical coherences and taking a formal statistical average over the fluctuating phases [18]. This procedure results in a system of equations that, when solved, yields the observed signals.

From the density matrix of the final state, one can obtain the fluorescence intensities of a given polarization along the unit vector \mathbf{e} from [19, 20, 21]:

$$I(\mathbf{e}) = \tilde{I}_0 \sum_{g_i, f_i, f_j} d_{g_i f_j}^{(ob)*} d_{e_i g_i}^{(ob)} \rho_{f_i f_j}, \quad (2)$$

where \tilde{I}_0 is a constant and $d_{g_i f_j}^{(ob)} = \langle g_i | \mathbf{d} \cdot \mathbf{e} | f_j \rangle$ is the matrix element between the ground and final states of the dipole operator along a specific polarization direction \mathbf{e} , i.e., the x - or y - direction.

III. CALCULATION OF SCALAR AND TENSOR POLARIZABILITIES

A. Motivation

The description of the signals obtained from the experiment described above depends on two atomic properties simultaneously: the hyperfine constant A and the tensor polarizability α_2 . If one of these constants can be known by independent means, the experiment provides a way to determine the other. In this section, we describe an all-order relativistic many-body calculation of the tensor polarizability α_2 . A reliable theoretical estimate of this constant, together with the experimental results of the previous section, can be used to estimate the hyperfine constant A , which is difficult to calculate theoretically and has not been measured to high precision for the 7,9, and 10 $D_{5/2}$ states of cesium.

B. Method

The scalar α_0 and tensor α_2 polarizabilities of an atomic state v are calculated using formulas

$$\alpha_0 = \frac{2}{3(2j_v + 1)} \sum_n \frac{\langle n || D || v \rangle^2}{E_n - E_v} \quad (3)$$

$$\alpha_2 = -4 \left(\frac{5j_v(2j_v - 1)}{6(j_v + 1)(2j_v + 1)(2j_v + 3)} \right)^{1/2} \sum_n (-1)^{j_v + j_n + 1} \begin{Bmatrix} j_v & 1 & j_n \\ 1 & j_v & 2 \end{Bmatrix} \frac{\langle n || D || v \rangle^2}{E_n - E_v}, \quad (4)$$

where D is the dipole operator and the formula for α_0 includes only the valence part of the polarizability. The contribution to α_0 from the ionic core is negligible for the present calculation ($16 a_0^3$). The sum over n includes the $nP_{1/2}$, $nP_{3/2}$, and $nF_{5/2}$ states for the calculation of the $D_{3/2}$ polarizabilities in cesium and the $nP_{3/2}$, $nF_{5/2}$, and $nF_{7/2}$ states for the calculation of the $D_{5/2}$ polarizabilities. The sum over the intermediate states n converges rather quickly and only the first few terms need to be calculated accurately. Therefore, we separate the calculation of the polarizabilities into the calculation of the main term α^{main} and the evaluation of the remainder α^{tail} . We include the contributions from the following states into the main term: $6P$, $7P$, $8P$, $9P$, $10P$, $11P$, $12P$, $4F$, $5F$, $6F$, $7F$, and $8F$ to calculate the polarizabilities of all D states considered in this paper. We also include the contributions from the $9F$ states into the calculation of the $\alpha^{\text{main}}(10D)$. All electric-dipole reduced matrix elements in Eqs. (3, 4) that are needed for the calculation of the main term are calculated using the relativistic all-order method, which is briefly described below. We use experimental energies from [22] in the main term calculations. We note that the polarizabilities of the $9D - 10P$ and $10D - 11P$ energy differences, respectively, since they are small ($50 - 100 \text{ cm}^{-1}$). We assume that the energies in Ref. [22] are accurate to all quoted digits. The remainders α^{tail} are small for all sums and are calculated in the Dirac-Hartree-Fock (DHF) approximation.

The all-order method used here sums infinite sets of many-body perturbation theory terms. We refer the reader to Refs. [23, 24, 25] for a detailed description of the approach. Briefly, the wave function of the valence electron v is represented as an expansion

$$|\Psi_v\rangle = \left[1 + \sum_{ma} \rho_{ma} a_m^\dagger a_a + \frac{1}{2} \sum_{mnab} \rho_{mnab} a_m^\dagger a_n^\dagger a_b a_a + \sum_{m \neq v} \rho_{mv} a_m^\dagger a_v + \sum_{mna} \rho_{mnva} a_m^\dagger a_n^\dagger a_a a_v \right] |\Phi_v\rangle, \quad (5)$$

where Φ_v is the lowest-order atomic state function, which is taken to be the *frozen-core* Dirac-Hartree-Fock wave function of a state v . This lowest-order atomic state function can be written as $|\Phi_v\rangle = a_v^\dagger |0_C\rangle$, where $|0_C\rangle$ represent DHF wave function of a closed core. The indices m and n designate excited states and indices a and b designate core states. The equations for the excitation coefficients are solved iteratively until the correlation energy converges to an acceptable accuracy. The excitation coefficients ρ_{ma} , ρ_{mv} , ρ_{mnab} , and ρ_{mnva} are used to calculate the matrix elements, which can be expressed in the framework of the all-order method as linear or quadratic functions of the excitation coefficients. The electric-dipole matrix elements as well as the hyperfine constants are calculated using the same approach. The expansion given by Eq. (5) is restricted to single and dou-

ble (SD) excitations leading to the omission of certain fourth- and higher-order terms.

We use B-splines [26] to generate a complete set of DHF basis orbitals for the all-order calculation. Here, we use $N = 70$ splines for each angular momentum. The basis orbitals are constrained to a cavity of radius $R = 220$ a.u. The size of the cavity is taken to be large enough to fit all of the states needed for the calculation of the main terms for all of the polarizabilities calculated in this work. The calculation of the polarizabilities of the $9D$ and $10D$ states requires such a large cavity since we need to be able to properly describe states up to $12P$ and $9F$. This work required extensive study of the numerical accuracy and stability of the calculations. We verified that our basis set gives correct lowest-order (DHF) values for the energies of all relevant states and transition matrix elements between these states. We have also verified that our basis set correctly reproduces DHF values of the hyperfine constants for all the nD_J states considered here. We find that it is necessary to use 70 splines to produce an accurate basis set. We also conducted an all-order calculation with a smaller cavity ($R = 90$ a.u.) that is appropriate for the calculation of the properties of the low-lying states and found that the properties of the low-lying states are accurately described by our large $R = 220$ a.u., $N = 70$ basis set. Therefore, we conclude that numerically accurate results can be obtained even for such highly-excited states as $12P$ with the use of large basis sets.

C. Results

The contributions to the scalar and tensor polarizabilities for the $7D_{3/2}$ state in cesium are listed in Table I. We note that the calculation of the scalar and tensor polarizability differs only in the angular factor, and all matrix elements and energies are the same. The corresponding energy differences and the absolute values of the lowest-order and final all-order electric-dipole reduced matrix elements are also listed. The energy differences are given in cm^{-1} . Electric-dipole matrix elements are given in atomic units (ea_0), and polarizabilities are given in $10^3 a_0^3$, where a_0 is the Bohr radius. The difference between the lowest-order values and the all-order values allows to evaluate the size of the correlation correction. The accuracy of our calculation is generally higher when the relative size of the correlation correction is smaller.

The contributions from all terms in α^{main} are listed separately to identify the most important terms. The remainder α^{tail} is separated to $\alpha^{\text{tail}}(nP_{1/2})$, $\alpha^{\text{tail}}(nP_{3/2})$, and $\alpha^{\text{tail}}(nF_{5/2})$ for the study of the convergence of these three sums.

We find that three contributions, from the $8P_{1/2}$, $8P_{3/2}$, and $5F_{5/2}$ states, are dominant. Another term ($4F_{5/2}$) gives a small but significant contribution to the tensor polarizability. Therefore, we conduct a more accurate calculation of the relevant matrix elements and

TABLE I: The contributions to scalar and tensor polarizabilities for the $7D_{3/2}$ state in cesium. The corresponding energy differences and the absolute values of the lowest-order (DHF) and final all-order electric-dipole reduced matrix elements are also listed. The energy differences are given in cm^{-1} . The electric-dipole matrix elements are given in atomic units (ea_0), and the polarizabilities are given in $10^3 a_0^3$, where a_0 is Bohr radius.

Contribution	nlj	$Z_{nlj,7D_{3/2}}^{DHF}$	$Z_{nlj,7D_{3/2}}^{SD}$	$E_{nlj} - E_{7D_{3/2}}$	$\alpha_0(7D_{3/2})$	$\alpha_2(7D_{3/2})$
$\alpha^{\text{main}}(nP_{1/2})$	$6P_{1/2}$	1.628	2.067	-14869.6	-0.011	0.011
	$7P_{1/2}$	4.030	6.580	-4282.2	-0.370	0.370
	$8P_{1/2}$	33.633	31.970	-338.7	-110.4(1.2)	110.4(1.2)
	$9P_{1/2}$	13.535	8.734	1589.4	1.756	-1.756
	$10P_{1/2}$	3.843	2.819	2679.2	0.109	-0.109
	$11P_{1/2}$	2.026	1.537	3355.8	0.026	-0.026
	$12P_{1/2}$	1.324	1.020	3805.0	0.010	-0.010
$\alpha^{\text{tail}}(nP_{1/2})$					0.041	-0.041
$\alpha^{\text{main}}(nP_{3/2})$	$6P_{3/2}$	0.794	0.983	-14315.5	-0.002	-0.002
	$7P_{3/2}$	2.111	3.336	-4101.2	-0.099	-0.079
	$8P_{3/2}$	15.190	14.351	-256.1	-29.4(3)	-23.5(3)
	$9P_{3/2}$	5.590	3.430	1634.1	0.263	0.211
	$10P_{3/2}$	1.642	1.142	2706.1	0.018	0.014
	$11P_{3/2}$	0.872	0.627	3373.2	0.004	0.003
	$12P_{3/2}$	0.572	0.417	3816.9	0.002	0.001
$\alpha^{\text{tail}}(nP_{3/2})$					0.008	0.006
$\alpha^{\text{main}}(nF_{5/2})$	$4F_{5/2}$	9.165	13.027	-1575.4	-3.9(1)	0.79(3)
	$5F_{5/2}$	46.603	43.406	923.7	74.6(1.1)	-14.9(2)
	$6F_{5/2}$	9.074	1.289	2281.9	0.027	-0.005
	$7F_{5/2}$	5.484	1.999	3100.4	0.047	-0.009
	$8F_{5/2}$	3.767	1.695	3631.1	0.029	-0.006
$\alpha^{\text{tail}}(nF_{5/2})$					0.434	-0.087
Total					-66.8(1.6)	71.2(1.2)

evaluate their uncertainties. The study of the breakdown of the correlation correction demonstrates that the main contributions to these transitions come from the terms containing only single valence excitation coefficients ρ_{mv} (see Eq. (5)). In such cases, it is possible to use a semi-empirical scaling procedure such as is described, for example, in Ref. [24] to estimate dominant classes of the omitted higher-order corrections. The single excitation coefficients ρ_{mv} are multiplied by the ratio of the experimental and theoretical correlation energy, and the calculation of the matrix elements is repeated using the modified excitation coefficients. The difference between the *ab initio* and scaled SD all-order values for the particular matrix element is taken to be its uncertainty. The relative uncertainty of the corresponding contribution to polarizability is twice the relative uncertainty of the matrix element. As we noted above, we assume that the experimental energies are accurate to all digits quoted in Ref. [22]. The uncertainties of the total polarizability values are obtained by adding the uncertainties of the individual terms in quadrature. The uncertainty in all remaining contributions is estimated to be insignificant in comparison with the uncertainty of the dominant terms. We observe significant cancellations between the dominant terms for both scalar and tensor polarizabilities of the $7D_{3/2}$ state. However, the cancellation is more severe

for the scalar polarizability, where the contributions from $8P_{1/2}$ and $5F_{5/2}$ states are comparable in size but have opposite signs. Therefore, we expect higher accuracy of our tensor polarizability calculation in comparison with the scalar one.

The contributions to scalar and tensor polarizabilities for the $7D_{5/2}$ state in cesium are listed in Table II. The table is structured in exactly the same way as the one for the $7D_{3/2}$ state. We find that the contribution from the $8P_{3/2}$ state is clearly dominant and the cancellation is much less severe. For the tensor polarizability, the next largest term, $5F_{7/2}$, is six times as small as the dominant term. The accuracy of the matrix elements in the dominant terms is similar for the $7D_{3/2}$ and $7D_{5/2}$ states. Therefore, our calculation of the $7D_{5/2}$ polarizabilities is expected to be more accurate than that of the $7D_{3/2}$ polarizabilities.

The contributions to scalar and tensor polarizabilities for the $9D_J$ and $10D_J$ states in cesium are listed in Tables III and IV, respectively. The breakdown of the polarizability contributions is similar to that of the $7D$ polarizability calculations. We list only the dominant contributions separately and group all of the other contributions together in the rows labeled ‘‘Other’’. The uncertainty is evaluated using the method described above. The relative importance of the correlation corrections de-

TABLE II: The contributions to the scalar and tensor polarizabilities for the $7D_{5/2}$ state in cesium. The corresponding energy differences and the absolute values of the lowest-order (DHF) and the final all-order electric-dipole reduced matrix elements are also listed. The energy differences are given in cm^{-1} . The electric-dipole matrix elements are given in atomic units (ea_0), and the polarizabilities are given in $10^3 a_0^3$.

Contribution	nlj	$Z_{nlj,7D_{5/2}}^{\text{DHF}}$	$Z_{nlj,7D_{5/2}}^{\text{SD}}$	$E_{nlj} - E_{7D_{5/2}}$	$\alpha_0(7D_{5/2})$	$\alpha_2(7D_{5/2})$
$\alpha^{\text{main}}(nP_{3/2})$	$6P_{1/2}$	2.375	2.909	-14336.5	-0.014	0.014
	$7P_{1/2}$	6.303	9.679	-4122.2	-0.554	0.554
	$8P_{1/2}$	45.594	43.210	-277.1	-164.3(1.7)	164.3(1.7)
	$9P_{1/2}$	16.835	10.774	1613.1	1.755	-1.755
	$10P_{1/2}$	4.939	3.555	2685.1	0.115	-0.115
	$11P_{1/2}$	2.623	1.947	3352.3	0.028	-0.028
	$12P_{1/2}$	1.720	1.294	3795.9	0.011	-0.011
$\alpha^{\text{tail}}(nP_{3/2})$					0.047	-0.047
$\alpha^{\text{main}}(nF_{5/2})$	$4F_{5/2}$	2.444	3.471	-1596.4	-0.184	-0.210
	$5F_{5/2}$	12.464	11.660	902.7	3.67(5)	4.20(5)
	$6F_{5/2}$	2.441	0.457	2260.9	0.002	0.003
	$7F_{5/2}$	1.472	0.590	3079.4	0.003	0.003
	$8F_{5/2}$	1.011	0.488	3610.1	0.002	0.002
$\alpha^{\text{tail}}(nF_{5/2})$					0.021	0.024
$\alpha^{\text{main}}(nF_{7/2})$	$4F_{7/2}$	10.925	15.292	-1596.5	-3.6(1)	1.28(4)
	$5F_{7/2}$	55.737	52.145	902.6	73.5(9)	-26.2(3)
	$6F_{7/2}$	10.926	2.049	2260.8	0.045	-0.016
	$7F_{7/2}$	6.588	2.643	3079.3	0.055	-0.020
	$8F_{7/2}$	4.522	2.186	3610.1	0.032	-0.012
$\alpha^{\text{tail}}(nF_{7/2})$					0.416	-0.148
Total					-89.0(1.9)	141.8(1.7)

TABLE III: The contributions to scalar and tensor polarizabilities for the $9D_{3/2}$ and $9D_{5/2}$ states in cesium in $10^3 a_0^3$.

Contribution	$\alpha_0(9D_{3/2})$	$\alpha_2(9D_{3/2})$
$10P_{1/2}$	-1760(9)	1760(9)
$10P_{3/2}$	-483(2)	-386(2)
$6F_{5/2}$	-129(2)	25.8(4)
$7F_{5/2}$	938(8)	-188(2)
Other	31	-22
Total	-1403(12)	1190(10)
Contribution	$\alpha_0(9D_{5/2})$	$\alpha_2(9D_{5/2})$
$10P_{3/2}$	-2653(12)	2653(12)
$7F_{5/2}$	46.3(3)	53.0(4)
$6F_{7/2}$	-117(2)	41.9(6)
$7F_{7/2}$	927(6)	-331(2)
Other	20	-30
Total	-1777(14)	2386(13)

TABLE IV: Contributions to the scalar and tensor polarizabilities for the $10D_{3/2}$ and $10D_{5/2}$ states in cesium in $10^3 a_0^3$.

Contribution	$\alpha_0(10D_{3/2})$	$\alpha_2(10D_{3/2})$
$11P_{1/2}$	-4995(24)	4995(24)
$11P_{3/2}$	-1379(6)	-1103(5)
$7F_{5/2}$	-425(2)	85.1(4)
$8F_{5/2}$	2478(16)	-496(3)
Other	84	-65
Total	-4236(29)	3416(24)
Contribution	$\alpha_0(10D_{5/2})$	$\alpha_2(10D_{5/2})$
$11P_{3/2}$	-7553(31)	7553(31)
$8F_{5/2}$	122(1)	140(1)
$7F_{7/2}$	-386(3)	138(1)
$8F_{7/2}$	2450(17)	-875(6)
Other	51	-89
Total	-5316(36)	6867(32)

creases with the principal quantum number n and the cancellation of different terms becomes less significant resulting in smaller uncertainties of the polarizabilities for the $9D$ and $10D$ states in comparison with the uncertainties for the $7D$ states. Overall, the uncertainties of our polarizability calculation are 0.5% – 2.3%.

D. Comparison with existing experimental values and other theory

Our results for the scalar polarizabilities of the $7D_J$, $9D_J$, and $10D_J$ states in cesium are compared with the experimental values from Refs. [10, 11, 12] and theoret-

TABLE V: Comparison of the scalar polarizabilities α_0 for the $7D$, $9D$, and $10D$ states in cesium with other theory and experiment. The polarizabilities are given in $10^3 a_0^3$.

State	This work	Expt.	Ref. [13]
$7D_{3/2}$	-66.8(1.6)	-60(8) [12]	-65.2
$9D_{3/2}$	-1403(12)	-1450(120) [11]	-1400
$10D_{3/2}$	-4236(29)	-4185(4) [10]	-4220
$7D_{5/2}$	-89.0(1.9)	-76(8) [12]	-87.1
$9D_{5/2}$	-1777(14)	-2050(100) [11]	-1770
$10D_{5/2}$	-5316(36)	-5303(8) [10]	-5300

TABLE VI: Comparison of the tensor polarizabilities α_2 for the $7D$, $9D$, and $10D$ states in cesium with other theory and experiment. The polarizabilities are given in $10^3 a_0^3$.

State	This work	Expt.	Ref. [13]
$7D_{3/2}$	71.2(1.2)	74.5(2.0) [4] 66(3) [12]	70.4
$9D_{3/2}$	1190(10)	1183(35) [4] 1258(60) [11]	1190
$10D_{3/2}$	3416(24)	3401(4) [10]	3410
$7D_{5/2}$	141.8(1.7)	129(4) [12]	140
$9D_{5/2}$	2386(13)	2650(140) [11]	2380
$10D_{5/2}$	6867(32)	6815(20) [10]	6850

ical values from Ref. [13] in Table V. The polarizabilities are given in $10^3 a_0^3$. The conversion factor from the $\text{MHz}/(\text{kV}/\text{cm})^2$ units to 10^3 atomic units used in the present work is $10^{-7}h/(4\pi\epsilon_0a_0^3) = 4.01878$, where h is the Planck constant. The present values agree with the experimental results for $7D_{3/2}$, $9D_{3/2}$, and $10D_{5/2}$ states within the corresponding uncertainties. There is some discrepancy with the accurate experimental value for the $10D_{3/2}$ state, but the discrepancy is only 1.5 of our estimated uncertainty. However, our values for the $7D_{5/2}$ and $9D_{5/2}$ states disagree significantly with the experimental values for these states. The calculations for the $7D_{5/2}$, $9D_{5/2}$, and $10D_{5/2}$ state polarizabilities are very similar. Thus, the experimental values for the scalar polarizabilities are not consistent with each other according to our theoretical model. Our calculations confirm the value for the $10D_{5/2}$ state to high precision, and one would have expected similar agreement in the case of the $7D_{5/2}$ and $9D_{5/2}$ state.

The results for the tensor polarizabilities for the $7D_J$, $9D_J$, and $10D_J$ states in cesium are compared with the experimental values from Refs. [4, 10, 11, 12] and theoretical values from Ref. [13] in Table VI. The polarizabilities are also given in $10^3 a_0^3$. The present results for the $nD_{3/2}$ states support the measurements of Refs. [4, 10] and disagree with the less precise previous measurements [11, 12]. The comparison of the $nD_{5/2}$ values with experiment mirrors the result of the comparison for the scalar polarizabilities: the $7D_{5/2}$ and $9D_{5/2}$ values differ significantly from the experiment while the $10D_{5/2}$

TABLE VII: The breakdown of the correlation correction to the hyperfine constants A for the $nD_{3/2}$ and $nD_{5/2}$ states in cesium calculated using the SD all-order method. The expressions for all terms are given in [23]. The values of the contributions for the dominant terms and total correlation correction are given in % relative to the lowest-order value for each state. The total contains contributions from all terms ($a - t$). The normalization factor is also listed.

Contribution	$5D_{3/2}$	$6D_{3/2}$	$7D_{3/2}$	$8D_{3/2}$	$9D_{3/2}$	$10D_{3/2}$
Term a	11%	26%	28%	28%	28%	28%
Term c	127%	57%	36%	28%	23%	21%
Term d	41%	9%	4%	2%	2%	1%
Term h	13%	9%	5%	4%	3%	3%
Term p	19%	13%	11%	10%	9%	9%
Total	214%	118%	87%	75%	69%	65%
Norm	1.10	1.14	1.12	1.10	1.10	1.09
Contribution	$5D_{5/2}$	$6D_{5/2}$	$7D_{5/2}$	$8D_{5/2}$	$9D_{5/2}$	$10D_{5/2}$
Term a	-352%	-264%	-228%	-213%	-205%	-200%
Term c	120%	54%	35%	27%	23%	21%
Term d	37%	8%	3%	2%	2%	1%
Term h	-154%	-28%	-5%	3%	6%	8%
Term n	18%	16%	14%	13%	12%	12%
Term p	13%	10%	9%	8%	8%	8%
Term r	-24%	-18%	-15%	-14%	-14%	-13%
Total	-339%	-217%	-184%	-171%	-164%	-160%
Norm	1.09	1.12	1.10	1.09	1.09	1.08

value agrees with the precise experiment within the corresponding uncertainties. Our values agree with the calculation of Ref. [13] for all states for both scalar and tensor polarizabilities.

IV. CALCULATION OF HYPERFINE CONSTANTS

In this section we evaluate the current knowledge about the hyperfine constants of the $D_{3/2}$ and $D_{5/2}$ states of cesium. We describe a calculation of the hyperfine constants for the $5D_{3/2} - 10D_{3/2}$ and $5D_{5/2} - 10D_{5/2}$ states of ^{133}Cs . Then we compare the results of the calculation to previously measured values. The calculation of the hyperfine constants also makes use of the relativistic all-order method and is done in the same way as the calculation of the electric-dipole matrix elements and with the same set of the excitation coefficients ρ_{ma} , ρ_{mv} , ρ_{mnab} , and ρ_{mnva} (see Eq. (5)). The breakdown of the correlation correction to the hyperfine constants A for $nD_{3/2}$ and $nD_{5/2}$ states in cesium calculated using the SD all-order method is given in Table VII. The expressions for the Terms a, c, d, h, n , and p are given in [23]. These terms are linear or quadratic functions of the excitation coefficients. The values of the contributions of the dominant terms and total correlation correction are given in % relative to the lowest-order value for each state. The normalization factor is also listed. We find that the correlation correction is very large, especially

TABLE VIII: The hyperfine constants A (MHz) for the $nD_{3/2}$ and $nD_{5/2}$ states in cesium. The lowest-order, “dressed” third-order values, and all-order values are compared with previous experiments. The experimental data are taken from [5].

State	DHF	Third order	All order	Expt. [5]
$5D_{3/2}$	18.2	47.0	52.3	48.78(7)
$6D_{3/2}$	9.27	21.5	17.8	16.30(15)
$7D_{3/2}$	4.70	10.1	7.88	7.4(2)
$8D_{3/2}$	2.65	5.46	4.20	3.94(8)
$9D_{3/2}$	1.63	3.28	2.51	2.35(4)
$10D_{3/2}$	1.07	2.12	1.62	1.51(2)
$5D_{5/2}$	7.47	-32.3	-16.4	-21.24(8)
$6D_{5/2}$	3.73	-8.15	-3.89	-3.6(10)
$7D_{5/2}$	1.88	-2.67	-1.42	-1.7(2)
$8D_{5/2}$	1.06	-1.15	-0.684	-0.85(20)
$9D_{5/2}$	0.651	-0.592	-0.384	-0.45(10)
$10D_{5/2}$	0.428	-0.343	-0.238	-0.35(10)

for the $D_{5/2}$ states where it is several times as large as the lowest-order value and has an opposite sign. Owing to such an enormous correlation correction, we do not expect our results to be very accurate for the $nD_{5/2}$ states. The scaling procedure described above or partial *ab initio* inclusion of the triple excitation as described in Ref. [25] can only evaluate corrections to terms c and d , that are not dominant for any of the states except $5D_{3/2}$. Therefore, we can not make an accurate estimate of the uncertainty of our values that is independent from experimental measurements.

Our results for the hyperfine constants A (MHz) for the nD state in Cs are compared with previous experiments in Table VIII. We list the lowest-order and “dressed” third-order values together with the SD all-order values. The “dressed” third-order calculation has all lowest-order matrix elements replaced by “dressed” matrix elements calculated in the random-phase approximation (RPA) [27]. We find large discrepancies between the third-order and all-order results indicating very large contributions from the fourth- and higher-order terms. Taking into account the very large size of the correlation correction and obviously large contributions from higher orders, we find that the agreement of the all-order calculation with measured values is remarkably good.

We have investigated the issue of the consistency of the experimental hyperfine data using our calculation. Table VII demonstrates that the breakdown of the correlation for the $6D-10D$ states is rather similar, especially for $nD_{3/2}$ states. We note that $nD_{3/2}$ and $nD_{5/2}$ states have to be considered separately. The distributions of the correlation for both $5D_{3/2}$ and $5D_{5/2}$ states are clearly very different from the ones for the other nD states, and these states are omitted from the consistency check below. For the $nD_{5/2}$ states, the relative contribution of Term h changes sign; however, the contribution from this term is small in comparison with the experimental un-

certainty. To cross-check the experimental data, we take the experimental value for one particular nD_J state and rescale it for all the other states with the same J using the theoretical values of the correlation corrections. The correlation correction is calculated as the difference between the final (experimental or theoretical) number and the lowest-order DHF value. For example, we take the experimental value $A_{6D_{3/2}}^{\text{Expt}}$ and determine how much we need to scale our theoretical correlation correction for the $6D_{3/2}$ state to obtain this value. The scaling factor is defined as

$$S(6D_{3/2}) = \frac{A_{6D_{3/2}}^{\text{Expt}} - A_{6D_{3/2}}^{\text{DHF}}}{A_{6D_{3/2}}^{\text{SD}} - A_{6D_{3/2}}^{\text{DHF}}},$$

where A^{DHF} and A^{SD} are the lowest-order and all-order values from Table VIII for the $6D_{3/2}$ state. Next, we take our theoretical value for another state, for example, $7D_{3/2}$, and rescale its correlation correction contribution using the scaling factor $S(6D_{3/2})$:

$$A(7D_{3/2}) = S(6D_{3/2}) \times \left(A_{7D_{3/2}}^{\text{SD}} - A_{7D_{3/2}}^{\text{DHF}} \right) + A_{7D_{3/2}}^{\text{DHF}}. \quad (6)$$

Then, we calculate $A(8D_{3/2})$, $A(9D_{3/2})$, and $A(10D_{3/2})$ using Eq. (6). We list these values in the column labeled $S(6D_{3/2})$ of Table IX which indicates that these values were obtained with the scaling factor $S(6D_{3/2})$. We repeat the procedure using other $nD_{3/2}$ values to define the scaling factor. The uncertainty of the rescaled values comes only from the experimental uncertainty of the initial experimental value $A_{nD_J}^{\text{Expt}}$. We find that all results in each row are consistent within the uncertainties, leading to the conclusion that the experimental results are internally consistent. We note that such a procedure will not be able to detect a systematic shift of all the experimental results. Since we cannot accurately evaluate the uncertainty of the scaling procedure itself, it is unclear if it can yield data that are more accurate than the corresponding experimental data, even though some of the rescaled data has smaller uncertainties than the actual experimental data. The accuracy of the rescaling is expected to be higher when Δn between the original and scaled state is the smallest.

V. ANALYSIS OF EXPERIMENTAL DATA AND ESTIMATE OF THE HYPERFINE CONSTANTS

The theoretical calculations of the hyperfine constants described in the previous section as well as the experimental measurements of [5] contained large uncertainties. The scaling procedure seems to indicate that the experimental values of the review [5], although taken from different sources, are consistent with each other. Thus, there is an indication that the scaling procedure could yield slightly more accurate predictions of hyperfine constants of states in adjacent levels if the hyperfine constant

TABLE IX: The consistency check of the experimental hyperfine constants A (MHz) values for the $nD_{3/2}$ and $nD_{5/2}$ states in cesium. The actual experimental data from Ref. [5] are listed in the second column. The columns labeled “ $S(nD_J)$ ”, $n = 6 - 10$, give data obtained by taking the experimental value for this particular nD_J state and rescaling it for all the other states using the theoretical values for the correlation correction as explained in the text. The uncertainty of the rescaled values comes only from the experimental uncertainty of the initial experimental value nD_J .

State	Expt. [5]	$S(6D_{3/2})$	$S(7D_{3/2})$	$S(8D_{3/2})$	$S(9D_{3/2})$	$S(10D_{3/2})$
$6D_{3/2}$	16.30(15)		16.5(5)	16.3(4)	16.2(4)	16.1(3)
$7D_{3/2}$	7.4(2)	7.33(6)		7.35(16)	7.3(1)	7.25(12)
$8D_{3/2}$	3.94(8)	3.93(3)	4.0(1)		3.92(7)	3.89(6)
$9D_{3/2}$	2.35(4)	2.36(2)	2.38(6)	2.36(5)		2.33(3)
$10D_{3/2}$	1.51(2)	1.53(1)	1.54(4)	1.53(3)	1.52(3)	
State	Expt.	$S(6D_{5/2})$	$S(7D_{5/2})$	$S(8D_{5/2})$	$S(9D_{5/2})$	$S(10D_{5/2})$
$6D_{5/2}$	-3.6(10)		-4.5(5)	-4.6(7)	-4.4(7)	-5.2(1.1)
$7D_{5/2}$	-1.7(2)	-1.3(4)		-1.7(4)	-1.6(3)	-2.0(5)
$8D_{5/2}$	-0.85(20)	-0.6(2)	-0.83(10)		-0.80(17)	-0.97(26)
$9D_{5/2}$	-0.45(10)	-0.34(14)	-0.47(6)	-0.48(11)		-0.56(16)
$10D_{5/2}$	-0.35(10)	-0.21(9)	-0.29(4)	-0.30(8)	-0.28(6)	

of one state is known. The experiment described in Section II could provide an independent cross-check of these findings.

With the tensor polarizabilities calculated in section III, the simulations described in section II can be used to estimate the hyperfine constant. First, we calculate a series of simulated curves, varying those experimental parameters that we cannot measure precisely, in particular the detuning of the lasers. When the overall shape of the simulated curve matches the experiment, the positions of the features depend on the values of the tensor polarizability α_2 and the hyperfine constant A .

We assume that the tensor polarizabilities calculated in section III for the 7,9, and $10D_{5/2}$ states of cesium are the most accurate values available because of the excellent agreement between the calculated and previously measured values for the $10D_{3/2}$ state of cesium. By fixing the tensor polarizability at the calculated value in our simulations, we can thus estimate the hyperfine constant A from the level-crossing signals in Figures 4, 5, and 6.

Table X summarizes the polarizabilities used in the simulations and the hyperfine values A obtained after a fit to the experimental data.

Considering the difficulty in calculating the hfs constants, the results of the relativistic many-body calculation for the hyperfine constant A agree reasonably well with the experimental measurements for the $7D_{5/2}$ and $9D_{5/2}$ states (within $\sim 1.5\sigma$). The large discrepancy in the case of the $10D_{5/2}$ state seems problematic, since the calculations should be internally consistent, if not completely reliable in absolute terms. This inconsistency could indicate that we slightly underestimated our uncertainties. It is also possible that the self-consistency check is less reliable in the case of the $nD_{5/2}$ states, because the DHF term and the all order term differ even in their sign.

VI. CONCLUSION

We obtained new values for the hfs constants A of the 7,9, and $10D_{5/2}$ states. Our values agreed with previously measured values, but achieved greater precision. The values were obtained by means of measured level-crossing signals, a detailed theoretical description of these signals, and values for the tensor polarizability calculated with an all-order relativistic many-body method. We demonstrated the all-order relativistic many-body method’s reliability even in highly excited states of ^{133}Cs by comparing scalar and tensor polarizabilities obtained by this method with previously experimentally measured values for the 7,9, $10D_{3/2}$ and 7,9, $10D_{5/2}$ states of ^{133}Cs .

Our calculated polarizability values were in good agreement with experiment except for the 7 and $9D_{5/2}$ states. However, the experimental values reported for these states are called into question by the fact that values reported in the same works for the $7D_{3/2}$ [12] and $9D_{3/2}$ [11] states also disagree with our calculations, whereas more recent measurements of the 7 and $9D_{3/2}$ states [4] support our calculation, as well as previous calculations [13]. The method was further applied to calculate values for the hyperfine constants A in the 5- $10D_{3/2}$ and 5- $10D_{5/2}$ states. Although the calculation cannot be considered reliable in absolute terms, nevertheless they agreed reasonably well in the case of the $7D_{5/2}$ and $9D_{5/2}$ states. For the $10D_{5/2}$ state, the agreement was not as good.

Acknowledgments

We would like to thank Walter Johnson for providing his “dressed” third-order code for the evaluation of the importance of higher orders for the hyperfine constant calculation. We thank Janis Alnis for help with the diode lasers and Robert Kalendarev for prepar-

TABLE X: Comparison of the experimentally obtained hyperfine constants with previous experiments and the theory presented in this work

Cesium atomic state	Calculated tensor polarizability ($10^3 a_0^3$)	hyperfine constant (MHz)		
		This work	Previous experiment	Theory
$7D_{5/2}$	141.8(1.7)	-1.56(9)	-1.7(2) [5]	-1.42
$9D_{5/2}$	2386(13)	-0.43(4)	-0.45(10) [5]	-0.384
$10D_{5/2}$	6867(32)	-0.34(3)	-0.35(10) [5]	-0.238

ing the cesium cells used in the experiment. The calculations of atomic properties were supported in part by DOE-NNSA/NV Cooperative Agreement DE-FC08-01NV14050. The work of MSS was supported in part by National Science Foundation Grant No. PHY-04-57078. The experimental measurements were supported by the

NATO SfP 978029 Optical Field Mapping grant, Latvian National Research Programme in Material Sciences Grant No. 1-23/50, and Latvian University Grant Y2-22AP02. K.B., F.G., and A.J. gratefully acknowledge support from the European Social Fund.

-
- [1] A. Khadjavi, J. Happer, W., and A. Lurio, *Phys. Rev. Lett.* **17**, 463 (1966).
- [2] A. Khadjavi, A. Lurio, and W. Happer, *Phys. Rev.* **167**, 128 (1968).
- [3] R. W. Schmieder, A. Lurio, and W. Happer, *Phys. Rev. A* **3**, 1209 (1971).
- [4] M. Auzinsh, K. Blushs, R. Ferber, F. Gahbauer, A. Jarmola, and M. Tamanis, *Opt. Commun.* **264**, 333 (2006).
- [5] E. Arimondo, M. Inguscio, and P. Violino, *Rev. Mod. Phys.* **49**, 31 (1977).
- [6] W. Hogervorst and S. Svanberg, *Physica Scripta* **12**, 67 (1975).
- [7] S. Svanberg and P. Tsekeris, *Phys. Rev. A* **11**, 1125 (1975).
- [8] S. Svanberg, P. Tsekeris, and W. Happer, *Phys. Rev. Lett.* **30**, 817 (1973).
- [9] B. R. Bulos, R. Gupta, G. Moe, and P. Tsekeris, *Phys. Lett. A* **55**, 407 (1976).
- [10] J. Xia, J. Clarke, J. Li, and W. A. van Wijngaarden, *Phys. Rev. A* **56**, 5176 (1997).
- [11] K. Fredriksson and S. Svanberg, *Z. Phys. A* **281**, 189 (1977).
- [12] J. E. Wessel and D. E. Cooper, *Phys. Rev. A* **35**, 1621 (1987).
- [13] W. A. V. Wijngaarden and J. Li, *J. Quant. Spect. Rad. Transf.* **52**, 555 (1994).
- [14] E. B. Aleksandrov, M. P. Chaika, and G. I. Khvostenko, in *Springer series on atoms and plasmas* (Springer, 1993).
- [15] S. Stenholm, *Foundations of laser spectroscopy* (Dover, Mineola, NY, 2005).
- [16] E. Arimondo, in *Progress in Optics, Vol 35* (Elsevier Science Publ B V, Amsterdam, 1996), vol. 35, pp. 257–354.
- [17] N. G. van Kampen, *Phys. Lett. C* **24**, 171 (1976).
- [18] K. Blush and M. Auzinsh, *Phys. Rev. A* **69**, 063806 (2004).
- [19] M. Auzinsh and R. Ferber, *Optical Polarization of Molecules* (Cambridge University Press, 2005).
- [20] J. P. Barrat and C. Cohen-Tannoudji, *J. Phys. Rad.* **22**, 329;443 (1961).
- [21] M. I. Dyakonov, *Sov. Phys. JETP* **20**, 1484 (1965).
- [22] C. E. Moore, *Atomic Energy Levels, NSRDS-NBS 35* (U. S. Government Printing Office, Washington DC, 1971).
- [23] S. A. Blundell, W. R. Johnson, Z. W. Liu, and J. Sapirstein, *Phys. Rev. A* **40**, 2233 (1989).
- [24] S. A. Blundell, W. R. Johnson, and J. Sapirstein, *Phys. Rev. A* **43**, 3407 (1991).
- [25] M. S. Safronova, W. R. Johnson, and A. Derevianko, *Phys. Rev. A* **60**, 4476 (1999).
- [26] W. Johnson, S. Blundell, and J. Sapirstein, *Phys. Rev. A* **37**, 307 (1998).
- [27] I. M. Savukov and W. R. Johnson, *Phys. Rev. A* **62**, 052512 (2000).